PAPER

Check for updates

Estimation of a stronger heparin binding locus in fibronectin domain III[14] using thermodynamics and molecular dynamics†

Sakshi Gupta,[a] Neha Tiwari,[a] Jyoti Verma,[b] Mohd Waseem,[b] Naidu Subbarao[b] and Manoj Munde 🔵[iD] *[a]

The HEP II (Heparin-binding site II) region of fibronectin (FN) containing domain III[14] plays a crucial role in cell adhesion and migration through heparin-binding on the cell surface. There are two such fibronectin heparin interacting peptide (FHIP I and FHIP II) sequences present in HEP II. However, the molecular principles by which these sites orchestrate heparin-binding processes are poorly understood. Such knowledge would have great implications in the therapeutic targeting of FN. With this aim, we have explored the binding studies of FHIP I and FHIP II with heparin using various biophysical methods. A fluorescence melting study specifically revealed the preference of heparin for domain III in FN, indicating the key contribution of FHIP I and FHIP II in heparin binding. In isothermal titration calorimetry (ITC), the higher binding affinity observed for FHIP II ($\sim 10^7$ mol^{-1}) compared to FHIP I ($\sim 10^6$ mol^{-1}) is expected due to the presence of a superior cluster of Arg and Lys residues in FHIP II, which can facilitate specific H-bonding interactions with heparin. Based on heat capacity changes, the key role of H-bonding, electrostatic and hydrophobic interactions was demonstrated in binding. Finally, the molecular docking and MD simulation results reinforced that the interaction of heparin (dodecasaccharide) is stronger and stable with the FHIP II peptide. The results described here suggest that these peptides provide all the structural and thermodynamic elements necessary for heparin-binding of HEP II of FN. Subsequently, it can be concluded that FHIP II could be a better location for therapeutic intervention in cell adhesion activity by FN.

Introduction

There is growing evidence that heparin-binding sites in the C-terminal domain of fibronectin (FN) participate in cell adhesion and migration through the recognition of heparin located on the cell surface.[1–3] This ability of FN plays a critical role in the development of several devastating pathologies including cancer and inflammation.[4] The heparin-binding sites of FN have populated in type III modules (12 to 14). The crystal structure of FN insinuated a distinctive basic patch in module III[14] of FN,[5] which also encompasses a well-known heparin-binding site II (HEP II), located within the carboxy-terminal of FN.[1] There is another site, HEP I, located in domain I of the N-terminus of FN.[6] However, the FN interactions with heparin are particularly dominated by the HEP II region.[7–10]

Heparin, a member of glycosaminoglycan (GAG) family, is often chosen as a model compound in the experimental studies of proteins and GAGs. It is highly negatively charged alternating copolymers containing uronic acid (L-iduronic acid or D-glucuronic acid) and D-glucosamine.[11] The presence of *N*-sulfamido, ester sulfate and uronic acid carboxylate groups results in high negative charge density. Over the years, several reports have been published on biophysical studies of protein–heparin interaction.[12–16] Interactions of several peptides such as cell penetrating peptides (CPPs) have also been reported with heparin.[17–21]

Since HEP II–heparin interactions can cause or exacerbates pathophysiological conditions,[22] there is a great prospect of developing agents that can block these interactions. However, there are multiple heparin-binding sites spread across HEP II, and in particular III[14] of FN, and therefore identifying the strongest heparin-binding site is critical for therapeutic intervention. For example, as shown in Fig. 1, FHIP I (203–210 sequence) is known to promote focal adhesion formation through heparin-binding,[1] and FHIP II (216–235) is another stretch involved in heparin interaction.[5] Despite the potential of FHIP I and FHIP II sites to bind heparin and drive FN function,

[a]School of Physical Sciences, Jawaharlal Nehru University, New Delhi-110067, India. E-mail: mundemanoj@gmail.com

[b]School of Computational and Integrative Sciences, Jawaharlal Nehru University, New Delhi-110067, India

† Electronic supplementary information (ESI) available. See DOI: 10.1039/d0ra01773f
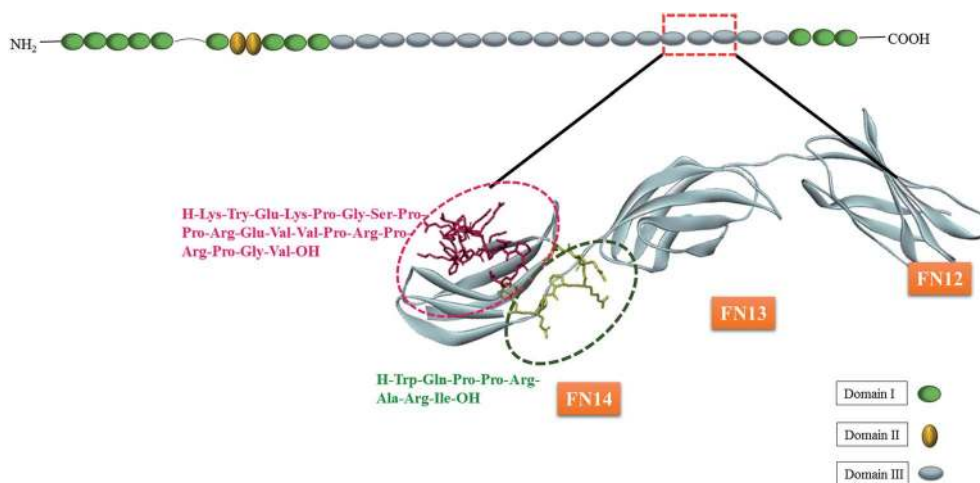
Fig. 1 At the top is the cartoon representation of FN with the three domains I, II and III. Also shown below is a zoomed out structure of FN12–14 units from domain III. The FHIP I and FHIP II peptides in the sub-domain 14 are displayed using sticks.

the thermodynamic assessment and molecular mechanism of their heparin-binding capabilities are elusive in literature.

To fulfill this goal, we have focused on both biophysical and computational tools to explore the interactions of heparin with FHIP I and FHIP II. Additionally, the results were also compared with the whole FN. Based on rigorous thermodynamic and MD simulation analysis, it was established that the interaction of heparin is stronger and stable with the FHIP II peptide. Subsequently, it was concluded that FHIP II could be a better location for therapeutic intervention in FN. Further, the knowledge gained here can be used to answer the fundamental question allied to the physical basis of the heparin–FN interaction. Also, the study may open a new approach to come up with broad-based peptide inhibitors against FN. Previously, it has been established that agents that block the protein–heparin interaction can be powerful therapeutic candidates.[14] A similar approach has also been adapted to carry out inhibition of protein–protein, protein–DNA complexes.[23] Additionally, such peptides also have applications as cell adhesive biomaterials.[24]

Materials and methods

Materials

Fibronectin from bovine plasma (MW 450 kDa), fibronectin (Adhesion Promoting) heparin interacting peptide (FHIP I), 8 amino acid sequence (H-Trp[203]-Gln[204]-Pro[205]-Pro[206]-Arg[207]-Ala[208]-Arg[209]-Ile[210]-OH) KI and heparin (13 kDa) from porcine intestinal mucosa were purchased from Sigma Aldrich. FHIP II, a 20 amino acid sequence (H-Lys[216]-Try[217]-Glu[218]-Lys[219]-Pro[220]-Gly[221]-Ser[222]-Pro[223]-Pro[224]-Arg[225]-Glu[226]-Val[227]-Val[228]-Pro[229]-Arg[230]-Pro[231]-Arg[232]-Pro[233]-Gly[234]-Val[235]-OH) was purchased from Integrated DNA Technologies. Amino acid residue number was followed according to a ref. 5. FN was dialyzed overnight in PBS, pH 7.4 at 4–5 °C. All the samples were prepared in 20 mM phosphate buffer containing 10 mM Na_2HPO_4, 10 mM NaH_2PO_4, 1 mM EDTA and 25 mM NaCl. The concentration of the protein was measured using absorbance at 280 nm on the UV-vis spectrophotometer. The

molar extinction coefficient used for FN, FHIP I and FHIP II were 580.5×10^3 M^{-1} cm^{-1}, 5690 M^{-1} cm^{-1} and 6354 M^{-1} cm^{-1} respectively. For pH dependent study at pH 4.0, 10 mM sodium acetate buffer was prepared using CH_3COONa, 1 mM EDTA and 25 mM NaCl. For 10 mM citrate buffer was prepared using 3.3 mM $HOC(COONa)(CH_2COONa)_2 \cdot 2H_2O$, 6.7 mM $C_6H_8O_7$, 1 mM EDTA and 25 mM NaCl.

Methods

ITC. ITC experiments were performed on MicroCal iTC200 system (Malvern Instruments Ltd., UK) at different temperatures at pH 7.4 and 4.0.[21,25,26] For all the experiments heparin was taken in the syringe and peptides were taken in the cell. At both the pHs, 1 mM heparin was titrated into 80 μM FHIP I. Another series of experiments were performed with FHIP II, where, 500 μM of heparin was titrated into 80 μM FHIP II. Experiments were done at both the pH under the temperature range of 15 to 35 °C. Citrate buffer was used to perform experiments at pH 4.0 as sodium acetate buffer leads to turbidity in case of FHIP II solution. The areas under these curves were determined by integration to yield the associated injection heats. The resulting corrected injection heats (lower panel) are plotted against the respective molar ratios. Heparin used in this study has the molecular weight of 15 kDa. The length of a single heparin molecule is expected to be 46 saccharide units. Stronger binding sites for FHIP I and FHIP II in ITC gives N (stoichiometry) around ~0.25, suggesting 4 peptides binding per 1 heparin molecule, which further gives estimate of about single peptide binding per ~11 (46/4) saccharides.

UV-vis spectroscopy. The UV measurements were performed in Cary 100 UV-vis spectrophotometer by titrating heparin into the fixed concentrations of FHIP I (100 μM) and FHIP II (100 μM) respectively. Titrations were performed at pH 7.4 and 4.0. Absorbance vs. concentration was plotted at $\lambda_{max} = 280$ nm to observe the effect of increased concentration heparin on the peptide absorbance.

Circular dichroism. Circular dichroism (CD) spectra were recorded on Chirascan Applied Photophysics CD spectrometer at 25 °C between wavelength range of 200 and 260 nm using a quartz cuvette 1 mm path length and 400 μL volume. Each spectrum is an average of 5 scans. The spectra of free heparin, free peptides and complex of heparin + peptide were taken.

Transmission electron microscopy (TEM). TEM micrographs were recorded using a transmission electron microscope (JEM-2100F JEOL) at an operating voltage of 200 kV.[26] Samples prepared in PBS buffer were drop cast on carbon-coated copper grid with 300 mesh size and dried. It was stained with uranyl acetate and dried again. The grid was placed in the sample compartment to record the micrographs.

Fluorescence spectroscopy. The fluorescence studies were performed using Cary Eclipse fluorescence spectrophotometer. Titrations were performed by the addition of heparin to FN in the presence and absence of KI. The samples were excited at 295 nm and emission spectra were recorded in the range of 300–400 nm. The excitation and emission slits were set at 10 nm and scan rate was 600 nm min^{-1}.

***In silico* molecular docking.** Computational studies were carried out to study the interaction of Hep-II domain of fibronectin with dodecasaccharide ([IdUA2S-GlcNS6S]$_6$) unit of Heparin. The dodecasaccharide was used based on stoichiometry of peptides (ten to twelve saccharides per peptide) observed in ITC. The structure files of the protein fibronectin (PDB: 1FNH) and dodecasaccharide (PDB: 1HPN) were downloaded from RCSB (https://www.rcsb.org/) for molecular docking. Fig. S3† provides an insight into the details of the structure of heparin used in MD simulation. The chosen heparin (dodecasaccharide) structure used in simulation consists of alternatively arranged six units of *N,O*6-disulfo-glucosamine (SGN) and six units of 2-*O*-sulfo-alpha-L-idopyranuronic acid (IDS). It contains all the features (such as a major repeating disaccharide unit with chemical functionalities) representative of a natural long chain of heparin. The same structure of heparin was used in molecular docking as well as in all MD simulations.

The interaction of heparin interacting peptide FHIP I and FHIP II in domain III[14] of the protein was studied with the dodecasaccharide unit. Since both the peptides are present in the III[14] domain therefore docking was carried out using this single domain of the protein. Molecular docking was performed using the GOLD software.[27] Protein was prepared by removing water molecules, and adding missing hydrogens. Hydrogen atoms were added to the ligand molecule using Open Babel software.[28] Two different docking experiments were performed by defining two different binding sites. First binding site corresponds to the FHIP I peptide and the second binding site is FHIP II. The resulting docked complexes were analysed using Pymol (https://pymol.org/2/).

Molecular dynamics simulation. Molecular dynamics (MD) simulation of a protein–ligand complex is carried out to analyze the molecular mechanics and stability of the complex. We performed molecular docking to identify the binding pose and affinity of the ligand with the protein molecule. Simulation studies were performed using GROMACS (version 2019.4).[29]

Different poses of the ligand were generated with the protein molecule (on both sites, FHIP I and FHIP II separately) and the highest ranking pose in accordance with the Gold score (docking score) was selected for further MD simulation.

First, the protein topology was generated using AMBER99SB force field and the ligand was parameterized by ACPYPE using general Amber force field (GAFF).[30,31] The complex was solvated using TIP3P water molecules and a cubic box was generated with 1.2 nm distance between the surface of the protein and the edge of the box. The whole system was solvated and neutralized by adding Na$^+$Cl$^-$ counter ions. Energy minimization was carried out using steepest descent and conjugate gradient methods to ensure no steric clashes or inappropriate geometry in the system. After the minimization, equilibration was done in two steps, in the first step *NVT* (*N* = number of particles, *V* = volume, and *T* = temperature) were kept constant and in the second, *NPT* (*N* = number of particles, *T* = temperature, and *P* = pressure) were constant throughout the simulation process. Finally, a 50 nanosecond (ns) simulations were performed for both the complexes. Different conformations of the ligand during the simulation at site FHIP I and FHIP II are shown in Fig. S4 and S5,† respectively. Since the ligand has many subunits, conformational change between the subunits may take place throughout the simulation process.

Results and discussion

Interaction of heparin with FHIP I

Thermodynamic characterization of the binding of heparin with FHIP I at pH 4.0 was performed using ITC (Fig. 2a–e). The binding thermograms were biphasic in nature at temperatures 15 °C, 20 °C and 25 °C, which gave a strong primary binding site and a weaker non-specific secondary binding site.[32] The data were best fitted using two sets of binding site model (Table 1). Although the data fitted consistently over the wide range of temperature for the primary binding mode (Fig. 2f), the secondary binding mode showed quite an unusual temperature dependence (Fig. 2g). At 35 °C and 40 °C, the secondary binding mode became less prominent, suggesting the loss of the non-specific interactions at a higher temperature. The primary binding mode was marked with a strong binding affinity (10^6 to 10^7 M^{-1} at 15 °C, 20 °C, 25 °C). At higher temperatures (30 °C and 35 °C), complexation was less favorable, resulting in ∼100 times lower binding affinity. The stoichiometry of binding (N_1) was observed in the range of 0.2–0.3 at all the temperatures, indicating 4–5 moles of FHIP I binding to 1 mole of heparin.

The ΔH_1 values are positive at lower temperatures (Fig. 2g) indicating that the complex formation is associated with electrostatic[33] and/or hydrophobic interaction.[34] The ΔH_1 values changed strongly from positive to negative with increase in temperature (Fig. 2f). At 25 °C, the binding is enthalpically as well as entropically driven. The negative increase in the entropy values illustrates that the hydrophobic interactions become less dominant with increasing temperature. The increase in negative enthalpy try to compensate this, however, the loss of entropy is much higher compared to gain in enthalpy resulting in a decrease in ΔG_1 with increasing temperature. Furthermore,
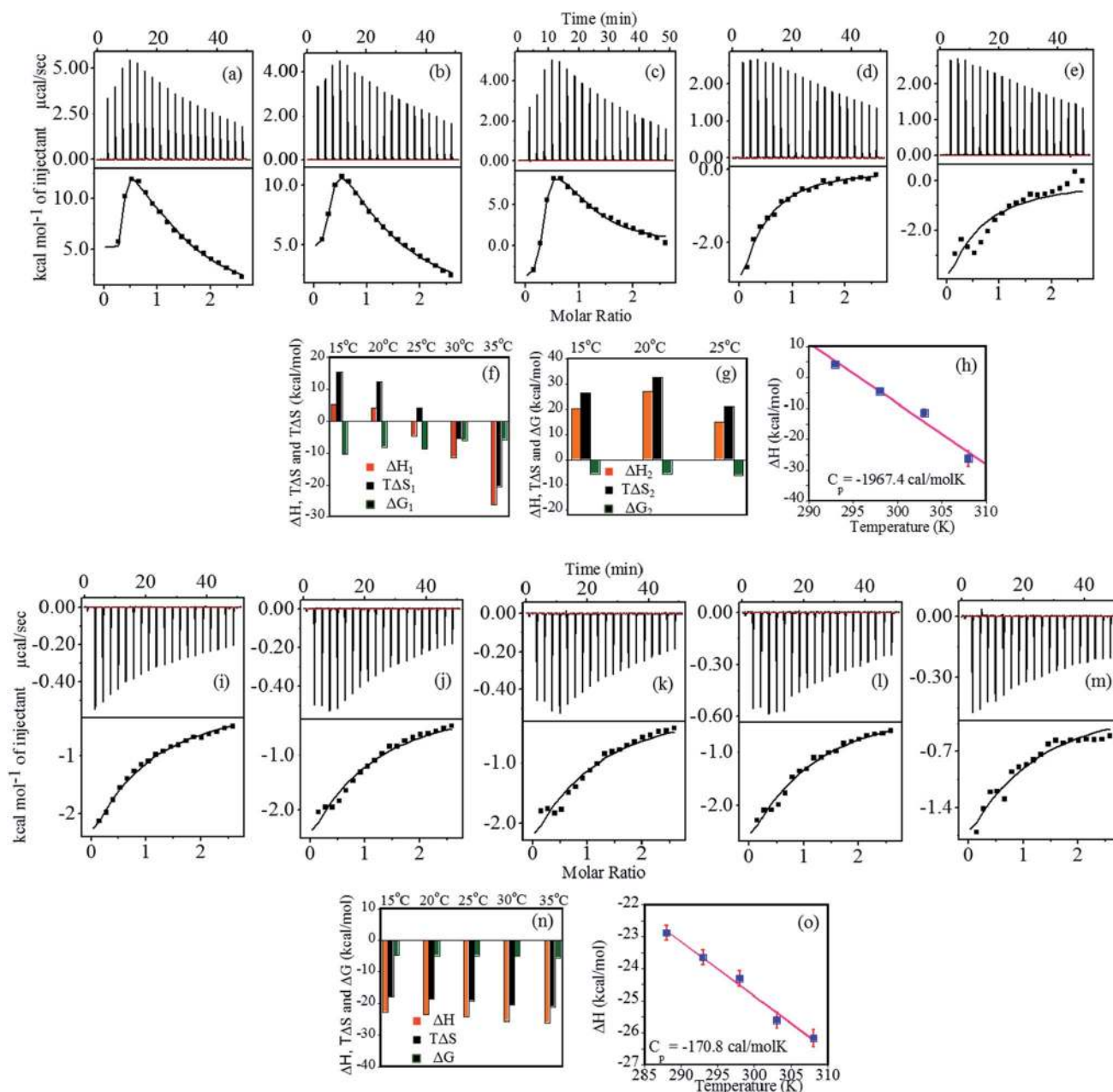
Fig. 2 (a–e) Top panel shows the ITC profile for binding of FHIP I (80 μM) to heparin (1 mM) at pH 4.0, indicating the sequential injection of heparin into FHIP I after correction of heat of dilution. Bottom panel shows the plot of integrated heat data, (f) bar diagram for parameters of primary binding site (g) bar diagram for parameters of secondary weak binding site, (h) heat capacity for the interaction of FHIP I with heparin obtained by linear squares fitting of the enthalpy data (■); ΔC_P value of −1967.4 cal mol^{-1} K^{-1} ($R = 0.985$), (i–m) top panel showing ITC profile for binding of FHIP I (80 μM) to heparin (1 mM) at pH 7.4. Bottom panel: plot of integrated heat data at temperature range of 288 K–308 K, (n) bar diagram showing the comparison of thermodynamic parameters at different temperatures. All the experiments were carried out using 25 mM NaCl and (o) linear squares fitting of the enthalpy data (■) at pH 7.4, which gives a ΔC_P value of −170.8 cal mol^{-1} K^{-1} ($R = 0.993$).

heat capacity change (ΔC_P) was obtained by the linear fitting of ΔH_1 *vs.* temperature (Fig. 2h). A large negative ΔC_P (−1967.4 cal mol^{-1} K^{-1}) is generally resulted when hydrophobic residues in water are transferred to a more nonpolar environment. This confirms the presence of dominant hydrophobic interactions at the binding interface.[35]

The enthalpy (ΔH_2) and entropy (ΔS_2) values were found to be positive with the overall binding driven mainly by entropy

(Fig. 2g). Thus, ΔG_2 resulted in negative values, although less favorable than ΔG_1. The non-sigmoidal curve associated with the binding of the peptide to the two different sets of sites often suggests the evidence of cooperativity. Thus, the binding of the peptide to the first set of sites energetically makes binding to the second set of sites less favorable which can be easily seen from ΔG_1 and ΔG_2 values, resulting in negative cooperativity.[36] Reduction in the stoichiometry (N) with a rise in temperature

Table 1 Thermodynamic parameters for the binding of FHIP I with heparin obtained from ITC at pH 4.0

Primary sites	N_1	ΔH_1 (kcal mol^{-1})	$T\Delta S_1$ (kcal mol^{-1})	$^a\Delta G_1$ (kcal mol^{-1})	$^aK_{A1} \times 10^6$ (M^{-1})
288 K	0.316 ± 0.01	5.20 ± 0	15.5	−10.3	66.0 ± 0
293 K	0.26 ± 0.01	4.251 ± 0.5	12.4	−8.1	1.2 ± 0.5
298 K	0.2 ± 0.01	-4.531 ± 0.7	4.23	−8.7	2.6 ± 1.41
303 K	0.23 ± 0.1	-11.4 ± 6.9	−5.4	−6.0	0.018 ± 0.004
308 K	0.20	-26.3 ± 3.5	−20.6	−5.7	0.01 ± 0.002
Secondary sites	N_2	ΔH_2 (kcal mol^{-1})	$T\Delta S_2$ (kcal mol^{-1})	ΔG_2 (kcal mol^{-1})	$K_{A2} \times 10^4$ (M^{-1})
288 K	1.08 ± 0.2	20.5 ± 5.5	26.3	−5.7	2.1 ± 0.98
293 K	0.9 ± 0.14	26.9 ± 5.3	32.5	−5.6	1.3 ± 0.2
298 K	0.83 ± 0.1	15.1 ± 2.8	21.3	−6.2	3.6 ± 0.9

^{a} Errors were about 15 to 20% in K_A and ΔG.

suggests an alteration in heparin–peptide interaction pattern at higher temperatures. The parameters obtained after fitting are shown in Table 2. The second binding phase, which disappeared at a higher temperature, must be driven by weaker hydrophobic interactions, whereas the first phase is consequence of strong, specific interactions from residues such as Arg and Glu.

The binding of FHIP I was further studied at pH 7.4 as shown in Fig. 2i–m. The binding parameters (Fig. 2n) were obtained using the single set of identical binding sites model. The binding affinity K_A was found to decrease slightly (5.6×10^3 M^{-1} to 4.4×10^3 M^{-1}) with an increase in temperature. N values were in the range of 0.19–0.27, suggesting that 4–5 molecules of peptide were bound to a single molecule of heparin (one peptide/10 saccharides) and the effect was independent of the temperature.[37] The much weaker binding affinity mostly suggests the presence of a non-specific binding mode resulted from hydrophobic interaction. The binding enthalpy (Fig. 2n) was found to be negative within the temperature range studied which indicates that the reaction was enthalpically driven. The ΔH values became slightly more negative (−22.88 to −26.17 kcal mol^{-1}) on increasing the temperature and the plot of ΔH vs. T yielded the very small negative value for ΔC_P (−170.8 cal mol^{-1} K^{-1}) from the slope of a linear least-squares fit ($R = 0.99$) (Fig. 2o).[38] Small negative ΔC_P indicates the contribution of hydrophobic interaction perhaps resulting in the burial of

non-polar amino acid residues within the peptide–heparin binding interface. This effect was more predominant at pH 4.0 with a negative ΔC_P value being almost 20 times higher than ΔC_P value at pH 7.4. It shows that hydrophobic interactions are a critical factor in the overall binding affinity of FHIP I.

The negative entropy shows unfavorable entropic contributions, which has an upward trend with the increasing temperature. This suggest that conformational entropy (negative contribution) must be dominant over solvation entropy (positive contribution).[36] The more negative enthalpic contributions overcome unfavorable entropic contributions, which makes ΔG negative and the reaction feasible. ΔG values showed only small variation with temperature where favorable enthalpy is compensated by unfavorable entropy.

The binding of heparin–FHIP I association was further studied by UV-absorbance studies. Absorbance spectrum of FHIP I was recorded over a wide range of wavelengths (200–300 nm) and changes at λ_{max} at 275 nm was observed on the addition of heparin at both the pHs (Fig. 3a–b). It was observed that binding of FHIP I with heparin resulted in a clear isosbestic point at 225 nm at pH 7.4, indicating the involvement of only one type of interaction, whereas, at pH 4.0, no clear isosbestic point indicates the presence the contribution of more than one type of interaction,[39] including possible nonspecific mode. This was supported by ITC in Fig. 2, where we found two types of complexes at pH 4.0. In Fig. 3c the plot of absorbance vs.

Table 2 Thermodynamic parameters for the association of FHIP I with heparin from ITC at pH 7.4

Temperature (K)	N	ΔH (kcal mol^{-1})	$T\Delta S$ (kcal mol^{-1})	ΔG (kcal mol^{-1})	$K_A \times 10^3$ (M^{-1})
288	0.25^b	-22.8 ± 0.4	−17.9	−4.9	5.6 ± 0.2
293	0.26 ± 0.75	-23.6^a	−18.6	−5.0	5.2 ± 2.8
298	0.25^b	-24.3 ± 1.6	−19.3	−5.0	4.9 ± 0.5
303	0.28 ± 0.67	-25.6^a	−20.5	−5.1	5.0 ± 2.2
308	0.2 ± 1.44	-26.1^a	−21.0	−5.1	4.4 ± 3.6

^{a} Errors were too large due to lack of initial data points in ITC fitting. ^{b} Errors not shown as parameter was constraint during fitting exercise.
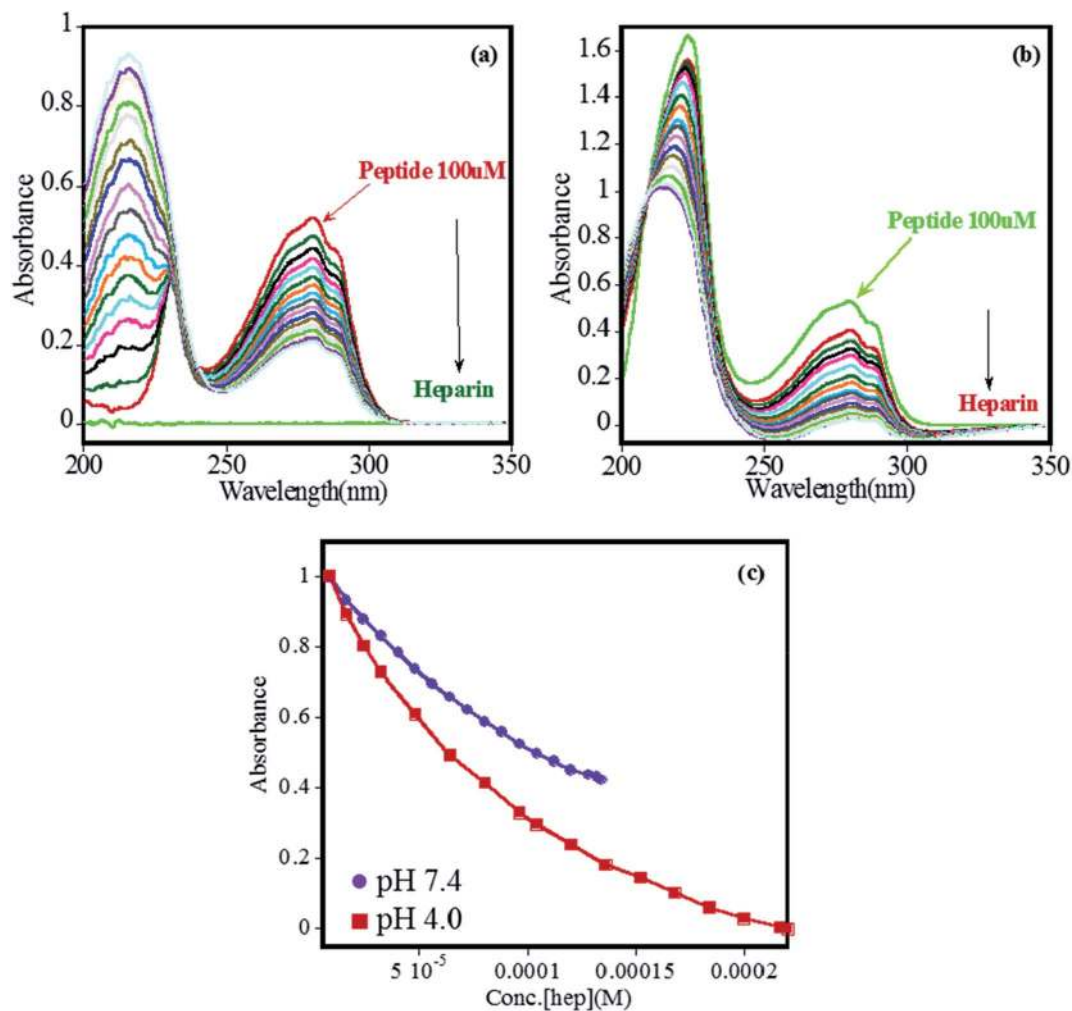
Fig. 3 UV-visible absorption titration for increasing concentration of heparin into 100 μM FHIP I in PBS buffer, NaCl 25 mM (a) at pH 7.4 (heparin 8–134 μM), (b) at pH 4.0 (heparin 8–220 μM) (c) absorbance vs. concentration plot for binding of heparin to 100 μM FHIP I (λ_{max} = 280 nm) ● pH 7.4, ■ pH 4.0.

concentration of heparin clearly suggests better binding at pH 4.0 compared to pH 7.4, in agreement with ITC.

Interaction of heparin with FHIP II

Interaction between FHIP II and heparin at pH 4.0 was performed using ITC at different temperatures (15 °C to 35 °C). Fig. 4a–e (upper panel) shows the representative raw ITC profiles resulting from the titration of FHIP II with heparin. Thermodynamic parameters are listed in Table 3. The binding enthalpy was found to be negative (−9.3 to −4.66 kcal mol^{-1}), which became less negative on increasing the temperature (Fig. 4f). The entropy ($T\Delta S$) value was slightly negative at 15 °C which turned more positive at a higher temperatures (−0.3 to 4.2 kcal mol^{-1}). The binding affinity (K_A) decreased slightly on increasing the temperature (7.0 × 10^6 M^{-1} to 2.45 × 10^6 M^{-1}). At 15 °C the reaction was enthalpically driven, whereas at higher temperatures it was enthalpically as well as entropically driven (Table 3). The ΔC_P obtained from Fig. 4g is +240.6 cal mol^{-1} K^{-1}. The positive heat capacity can be assigned to the exposure

of the hydrophobic groups to the aqueous environment upon complex formation. This also is a signature of electrostatic and specific H-bonding interaction driving the complex formation, which can be attributed to the presence of charged amino acids such as Arg and Lys in the FHIP II.

Fig. 4h–l represents the calorimetric profiles for binding between FHIP II and heparin (15 °C to 35 °C) at pH 7.4. The binding enthalpy was found to be negative at 15 °C, which became more negative (−10.8 to −32.8 kcal mol^{-1}) on increasing the temperature (Table 4). The $T\Delta S$ was also negative (−4.5 to −25.8 kcal mol^{-1}) accounting for the unfavorable entropic contributions. Thus the binding was basically dominated by favorable ΔH. The negative entropy suggested the role of conformational entropy, which restricted the rotational freedom of the heparin–FHIP II complex.[35] N value obtained was found to be 0.15, signifying that 6–7 molecules of FHIP II bind to 1 molecule of heparin. All the binding parameters are compared as shown in Fig. 4m. ΔC_P was determined to be negative (−1092.0 cal mol^{-1} K^{-1}) for the FHIP II attributing to the typical hydrophobic effects in the interactions (Fig. 4n). The
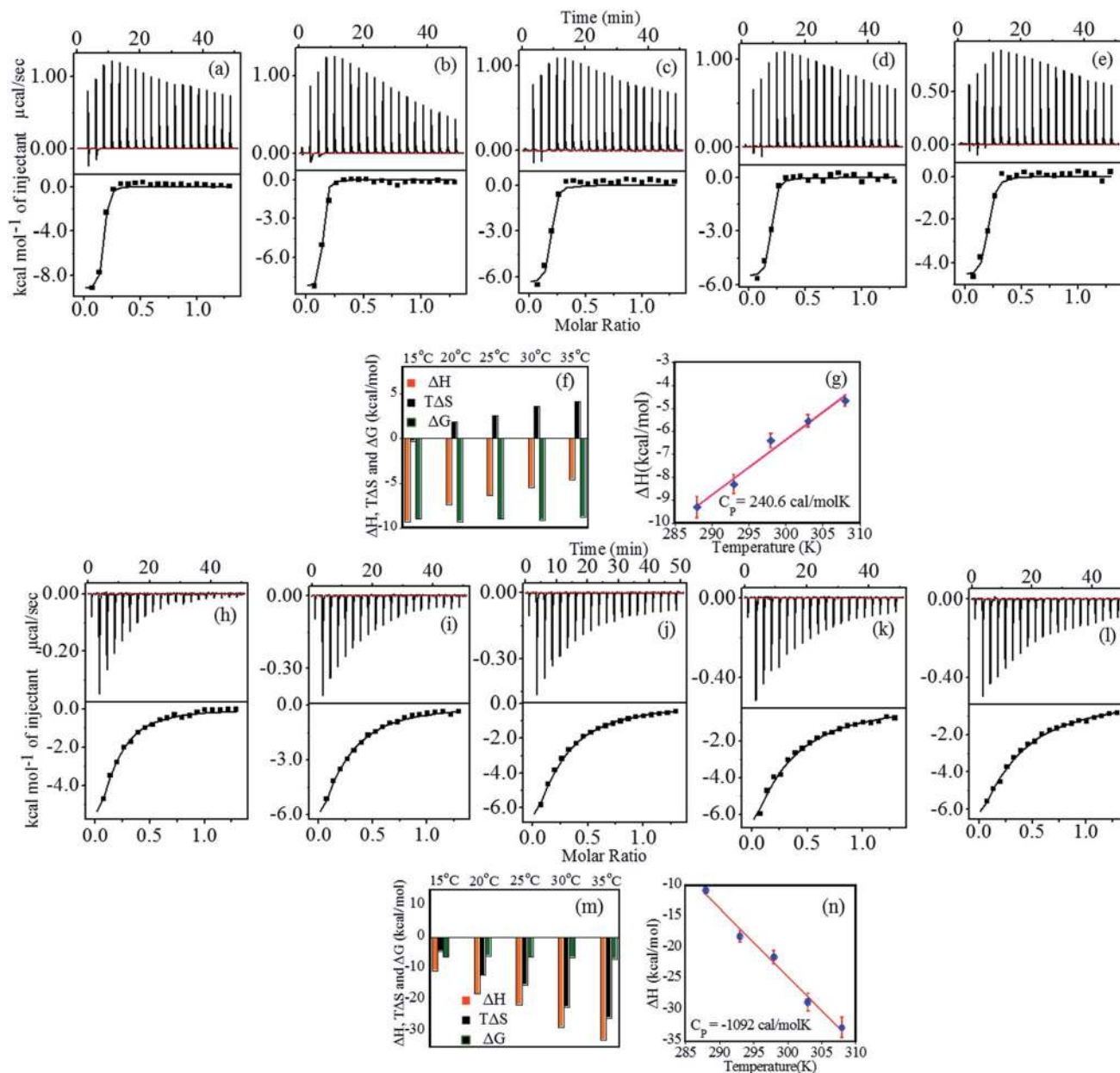
Fig. 4 (a–e) Top panel shows the ITC profile for binding of FHIP II (80 μM) to heparin (500 μM) at pH 4.0, indicating the sequential injection of heparin into FHIP II after correction of heat of dilution. Bottom panel shows the plot of integrated heat data at 288–308 K, (f) the bar diagram representation of thermodynamic parameters, (g) heat capacity plot for the interaction of FHIP II with heparin obtained by linear squares fitting of the enthalpy data (◆); ΔC_P value of +240.60.0 cal mol^{-1} K^{-1} ($R = 0.986$), (h–l) top panel showing ITC profile for binding of FHIP II (80 μM) to heparin (500 μM) at pH 7.4. Bottom panel: plot of integrated heat data at temperature range of 288–308 K, (m) bar diagram representation of thermodynamic parameters and (n) linear squares fitting of the enthalpy data (●) which gives a ΔC_P value of −1092.0 cal mol^{-1} K^{-1} ($R = 0.994$). All the experiments were carried out using 25 mM NaCl.

K_A and ΔG values showed very slight temperature dependence. The K_A at pH 7.4 is about 100 times lower than pH 4.0, which may have its origin in the possible role of electrostatic and hydrogen bonding interaction in the binding. A negative ΔC_P at pH 7.4 *versus* positive at pH 4.0 further supports this.

Here, since arginine and lysine have high pK_a (10 and 12, respectively),[12] and their side chains remain positively charged at pHs under study, these residues are unlikely to play any significant role in a decreased affinity of FHIP I and FHIP II at

pH 7.4 compared to 4.0. Therefore, to understand this further, we focused on the pH-dependent conformational status of free heparin using CD. It is evident from Fig. 5a that the free heparin showed a broad minimum between 208 nm and 214 nm, which is a clear sign of the presence of helical structures.[40] The helical content of heparin was found to be reduced at pH 7.4 compared to pH 4.0, which would suggest an alteration in heparin structure. Heparin is a negatively charged structure due to the presence of sulfate and carboxylate moieties, which gets

Table 3 Thermodynamic parameters for the association of FHIP II with heparin from ITC at pH 4.0

Temperature (K)	N	ΔH (kcal mol^{-1})	$T\Delta S$ (kcal mol^{-1})	$^a\Delta G$ (kcal mol^{-1})	^aK_A
288	0.15 ± 0.003	-9.3 ± 0.31	-0.3	-9.02	7.0×10^6
293	0.14 ± 0.01	-7.4 ± 0.67	1.9	-9.3	9.2×10^6
298	0.17 ± 0.006	-6.4 ± 0.38	2.6	-9.02	4.12×10^6
303	0.17 ± 0.004	-5.5 ± 0.22	3.6	-9.13	4.6×10^6
308	0.18 ± 0.006	-4.6 ± 0.25	4.2	-8.8	2.45×10^6

^{a} Errors were about 15 to 20% in K_A and ΔG.

Table 4 Thermodynamic parameters for the association of FHIP II with heparin from ITC at pH 7.4

Temperature (K)	N^b	ΔH (kcal mol^{-1})	$T\Delta S$ (kcal mol^{-1})	$^a\Delta G$ (kcal mol^{-1})	$^aK_A \times 10^4$
288	0.15	-10.8 ± 0.3	-4.5	-6.3	8.53 ± 0.56
293	0.15	-18.1 ± 0.3	-12.1	-6.0	4.08 ± 0.16
298	0.15	-21.5 ± 0.3	-15.2	-6.3	3.59 ± 0.09
303	0.15	-28.7 ± 0.7	-22.2	-6.5	2.38 ± 0.1
308	0.15	-32.8 ± 0.6	-25.8	-7.0	1.9 ± 0.06

^{a} Errors were about 15 to 20% in K_A and ΔG. ^{b} Errors not shown as parameters was constrained.

protonated at lower pH, resulting in more structured helical arrangement. An altered heparin conformation at pH 7.4 may be less suitable for its interaction with FHIP I or FHIP II, resulting in its reduced binding (Fig. 5b and c), also supported by ITC. Previously, a complete loss of binding for heparin was observed at extreme alkaline pH.[21] CD spectrum for free peptide around 200 nm showed the presence of a random coil structure (data not shown). Therefore, it can be concluded that the reduced intensity of CD spectrum of the FHIP I/FHIP II–heparin complex at higher pH (Fig. 5c) is due to the unfavorable conformation of heparin at that pH.[41]

The binding of heparin–FHIP II by UV-absorbance studies is shown in Fig. 6a–b. The presence of sharp isobestic points at pH 4.0 at 265 nm and 285 nm indicates the involvement of only one type of interaction.[39] On the contrary, at pH 7.4, there are no such isobestic points, indicating the presence of non-specific mode of binding between FHIP II and heparin. The higher binding capacity of FHIP II observed in Fig. 6c is in excellent agreement with ITC.

Interaction of heparin with FN

Due to the limited commercial availability of FN protein, we performed select experiments to get insights into its heparin-binding phenomenon. Fig. 7a displayed the CD spectra of free heparin and its complex with FN. The complex has a broad positive peak between 220 nm and 240 nm resulting from the involvement of intermolecular disulfide bonds present in the domain I and II as well as the two intramolecular disulfide bridges that connect the two fibronectin units.[40,42,43] CD of Free
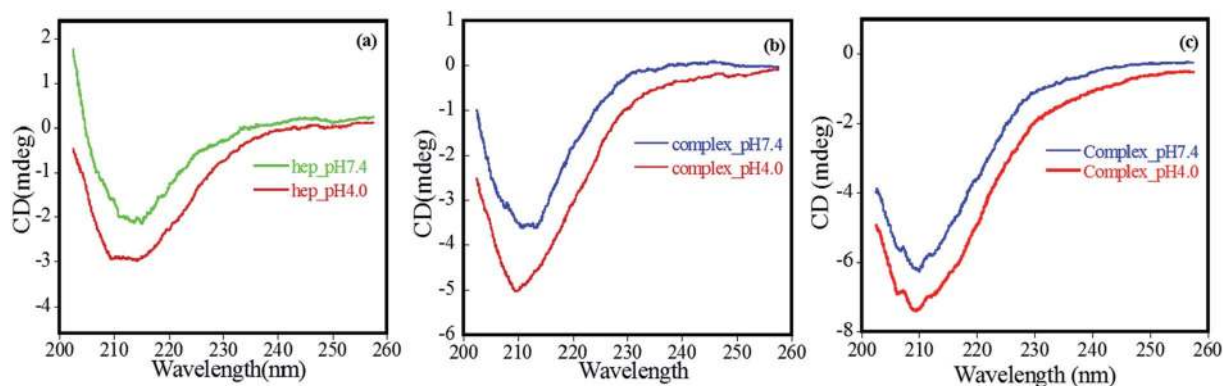

Fig. 5 CD spectrum carried from 200 nm to 260 nm at pH 4.0 and 7.4 for (a) heparin, (b) FHIP I–heparin complex and (c) FHIP II–heparin complex.
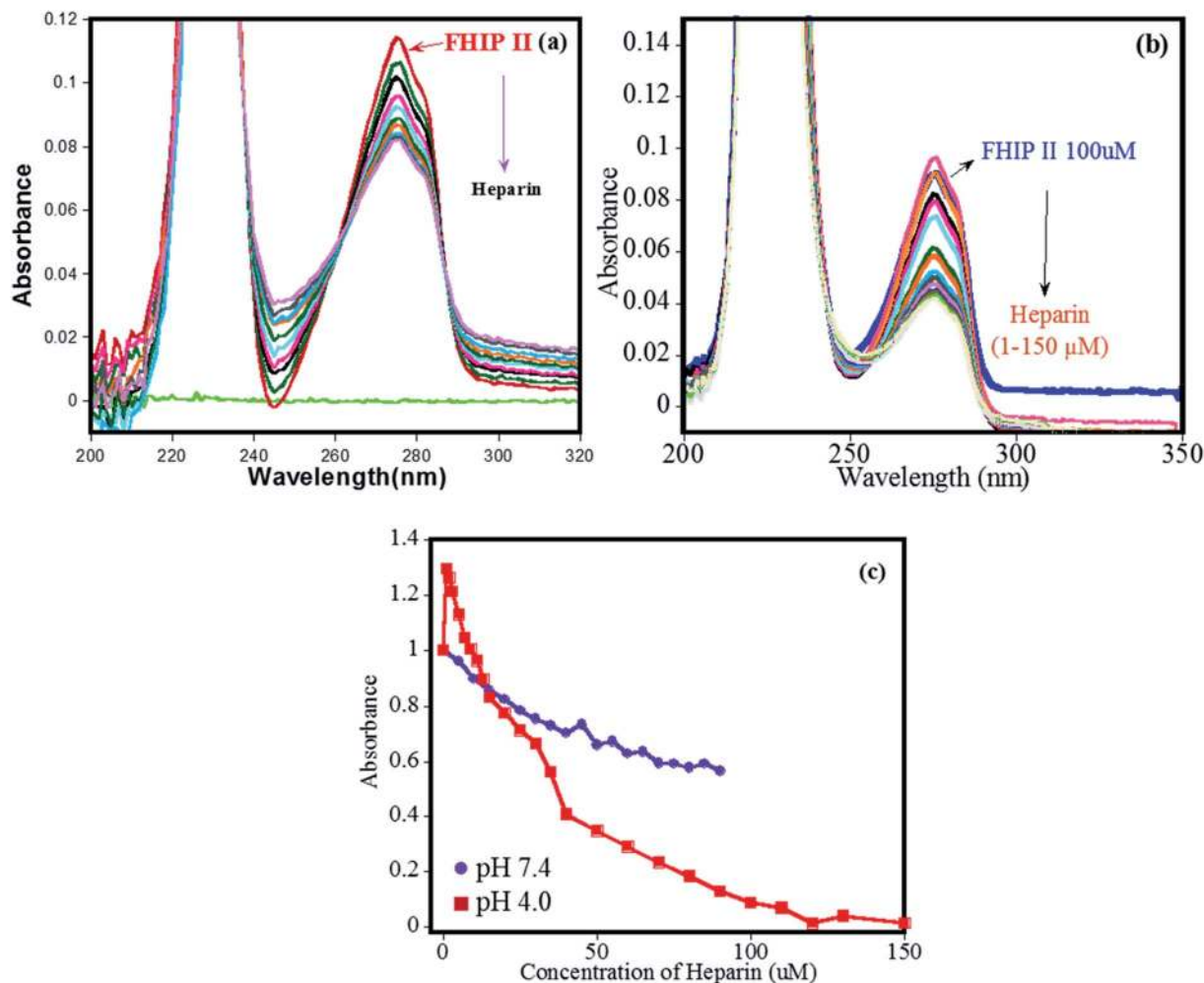
Fig. 6 UV-visible absorption titration for increasing concentration of heparin into FHIP II (a) pH 7.4 (heparin 1–90 μM) and (b) pH 4.0 (heparin 1–70 μM). (c) Absorbance *vs.* concentration plot for binding of heparin to FHIP II (λ_{max} = 280 nm) ● pH 7.4, ■ pH 4.0.

FN (Fig. 7b) showed a characteristic broad minimum between 212 and 218 nm, which arises due to the presence of β-structure in native FN.[44] The spectrum of heparin-bound FN, which was obtained by subtracting the spectrum of free heparin from the FN–heparin complex (Fig. 7b), was changed significantly, suggesting that heparin altered the structure of FN upon complex formation.[45] Also, the increase in the positive peak at 230 nm for heparin-bound FN indicates the stabilization of the disulfide group in FN as a result of heparin-binding.[46,47]

TEM micrographs were used to study the dimensions and shape of FN when complexed with heparin. Fig. 8a shows the view of FN molecules, which appear in the form of fibrils and exhibited folded domains on their extended arms. Images are also consistent with the previous structure of FN.[48] The TEM image of free heparin in Fig. 8b shows spherical morphology with the particle size in the range of 2–10 nm.[21] Interestingly, the FN on complexation with heparin showed a major change in protein morphology with the roughly embedded structures, which indicate that heparin molecules are bound to FN (Fig. 8c). Also, it can be seen that some of the heparin is in an unbound form.

Temperature-induced stability of FN in the presence of heparin

The melting studies of FN in the presence and absence of heparin gives two-step transition demonstrated using a plot of wavelength *vs.* temperature in Fig. 9. It implies that different domains of FN have different stability against temperature denaturation, which helped to distinguish the three domainial structures of FN. In the first transition (T_m = 52 °C), it shows a remarkable red shift from 329 nm to 343 nm with an increase of temperature, which could be due to Trp residues being exposed at a higher temperature. The absence of the disulfide linkages in the domain III makes it unstable towards increased temperature and thus chances of its unfolding are faster in the first transition, which enabled to distinguish the first transition as domain III of FN. Further increase in temperature led to a second (T_m = 63 °C) and third transition (T_m = 70 °C), which were more resistant towards protein unfolding.

In the presence of heparin, the melting temperature has shifted only for the first transition (lower) and for the third transition (higher). Since the first transition is designated as
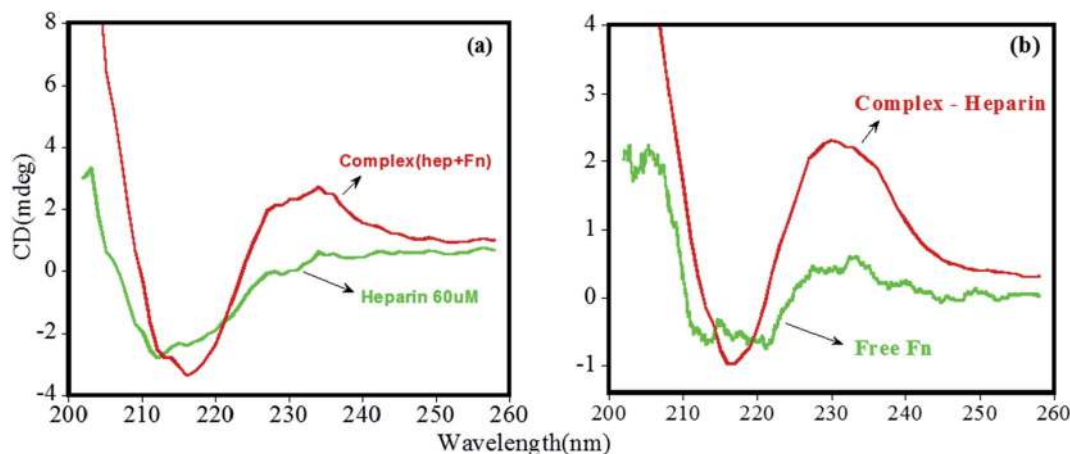
Fig. 7 CD spectrum showing conformational changes in the far UV range under the influence of pH (a) heparin, and FN + heparin complex, (b) free FN, and FN + heparin complex after subtracting the effect of free heparin.

domain III, the third transition should correspond to the domain I, as heparin is known to bind only a domain I and III of plasma FN. Thus, no changes were observed in the second transition of a protein in the presence of heparin, confirming the second transition belonging to domain II of the protein.

Mid-point of transition I (domain III) for free protein was observed at 335 nm and for a complex at 330 nm *i.e.* there is a blue shift in the emission spectra, indicating that the Trp in the domain III are buried in the hydrophobic environment, resulting into its more folded structure when heparin binds to FN. Since FHIP I and FHIP II are derived from domain III[14], it supports the fact that heparin is involved in specific interaction with this part of domain III. The binding affinity of heparin with FN was reported to be around $\sim 10^6$ mol^{-1}.[49] On the contrary, transition III (domain I) for free protein occurred at 347 nm and for complex occurred at 350 nm showing more exposed Try in domain I upon binding of heparin. In separate studies, it was reported that domain III (III[12,13,14]) of FN shows a maximum binding affinity for heparin.[50] To conclude, fluorescence melting suggested the strong interaction of heparin with domain III[14]. Interestingly, FHIP I and FHIP II sites are close to
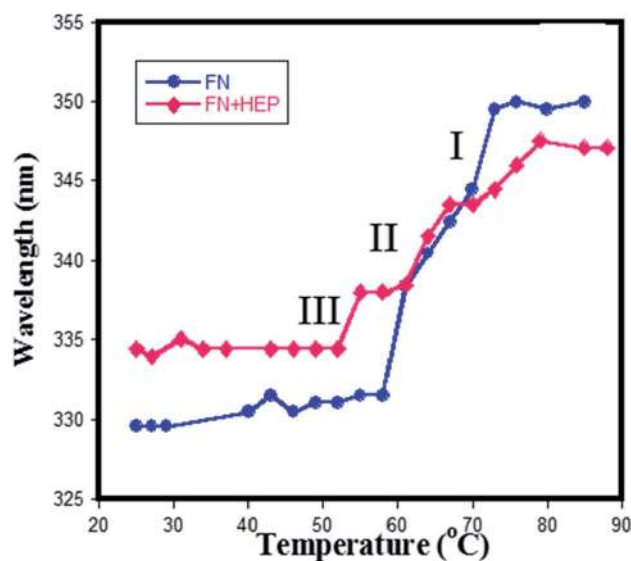

Fig. 9 Plot wavelength *vs.* temperature obtained from the melting of (◆) only FN (●) heparin–FN complex at pH 7.4.
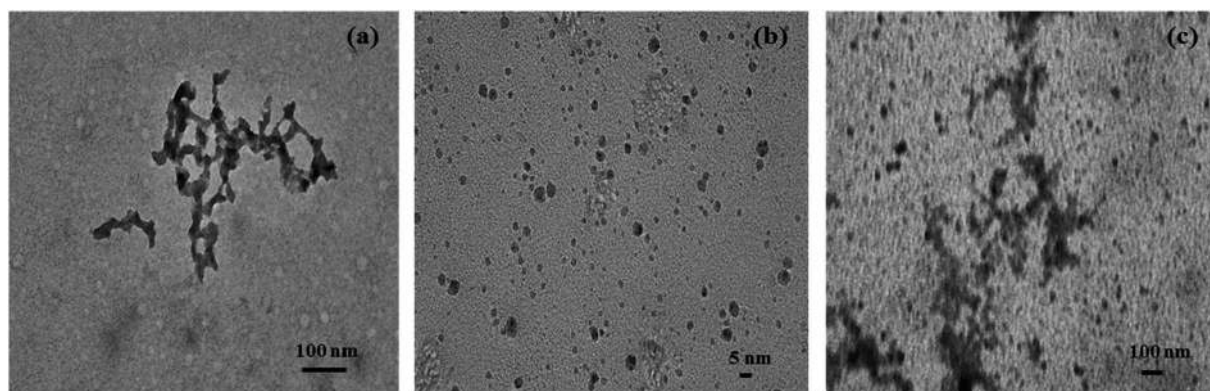

Fig. 8 TEM analysis of heparin–FN interaction. (a) FN (1 μM) alone showing the molecular architecture of native FN fibrils (b) heparin (1 μM) alone showing spherical morphology with a size range of 2–10 nm (c) FN–heparin complex showing large, roughly embedded structure of the FN.
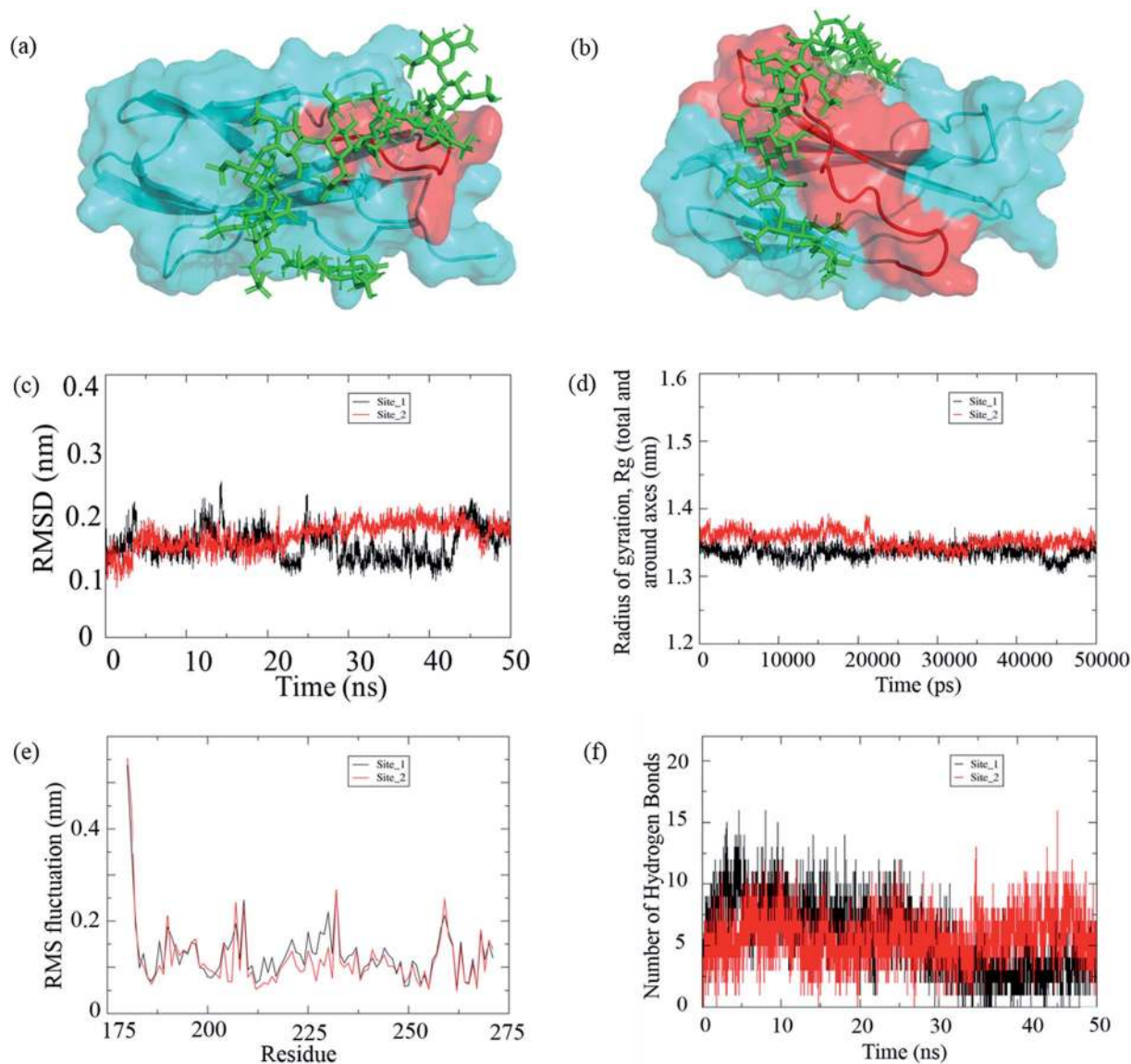
RSC Advances

Fig. 10 (a) Ligand (dodecasaccharide (PDB: 1HPN); green) bound to the F14 (PDB: 1FNH) domain with FHIP I shown in red as the active site, (b) ligand (dodecasaccharide; green) bound to the F14 domain with FHIP II shown in red as the active site; (c–f) molecular dynamics simulation of the complexes (c) RMSD of the two complexes, site 1 represents the complex with FHIP I as active site and site 2 represents the complex with FHIP II as the active site (d) radius of gyration (e) C-alpha RMSF graph and (f) hydrogen bonds between protein and ligand.

each other and may contribute to forming a single binding surface in III[14]. Thus, domain III[14] has two independent binding sites, which could be brought together promoting heparin binding.

KI quenching studies of FN were performed in the presence and absence of heparin (Fig. S1a, b, S2a and b†) to determine the surface accessibility of Trp in FN. FN quenching by KI gives lower K_{sv} values (Fig. S1c and Table S1†) in the absence of heparin, indicating that KI has limited access to Trp as all the Trp are buried inside the hydrophobic core of the protein.[51] In the presence of heparin, K_{sv} values do not change indicating that heparin-binding to FN does not lead to an overall change in the environment of Trp. As was also seen in the temperature-dependent study (Fig. 9), domain III folds, whereas domain I

partially unfolds as a result of heparin binding. This implies that Trp in domain I become partially exposed, and in domain III, they become buried upon heparin-binding. However, the average Trp exposure to a solvent remains the same, resulting in no change in the overall KI quenching.

Molecular docking and MD simulation

Based on experimental results, it was concluded that 10–12 saccharides bind per peptide molecule. Therefore, we used dodecasaccharide structure available in PDB to perform its molecular docking study with two different sites (FHIP I and FHIP II) in fibronectin Hep-II domain. The GOLD software was used to predict the docking scores of the complexes. The GOLD score for the site 1 (FHIP I) and site 2 (FHIP II) was 49.14 and

72.12, respectively. The protein–ligand complexes were analyzed using Pymol. Fig. 10 shows the docking pose of the ligand (dodecasaccharide) with FHIP I (Fig. 10a) and FHIP II (Fig. 10b).

It is well known that accurately describing the bimolecular interactions using computational techniques are difficult, which needs an excellent atomic-level understanding of the system. Often, the choice of force field parameters during MD simulation may affect the predicted structural properties. The limitations of the molecular mechanics force field still exist. They lack the ability to accurately capture subtle and weak interactions in the biomolecules to determine correct distribution of conformational ensembles. Usually in a biological system, the ligand-free binding pocket of protein is occupied by water molecules with few hydrogen bonds resulting in imperfect hydration of the critical residues. These water molecules are modulated during ligand binding. Hence, the solvent water has major impact on ligand binding and energetics.[52] We have used the TIP3P model in our study along with the AMBER force filed. The water model is a 3-point model having an angle of 104.5° with a rigid geometry matching that of actual water molecules. However, this model is suitable for simulation while using the AMBER99SB force field.[53]

In order to confirm and compare the stability of both the complexes, we carried out a MD simulation of 50 ns, and the protein–ligand complex stability throughout the trajectory was analyzed. After running a 50 ns simulation for both the complexes, it was observed that the complexes were stable and reached a plateau. Also, we could find a consistency with the experimental results; hence, we stopped at 50 ns simulation time. The root mean square deviation (RMSD) for the complex with site 1 (FHIP I) shows deviations between 20 to 40 ns whereas, the site 2 (FHIP II) complex shows relatively stable graph throughout the 50 ns simulation (Fig. 10c and S6†). The radius of gyration (R_g) is the measure of structural stability and compactness of the protein. The R_g value for the protein was between 1.3 nm to 1.4 nm for both the complexes (Fig. 10d). In the initial trajectory analysis, we found that the RMSD and the gyration time plot had reached a plateau. Therefore, the comparison between these complexes could be reliable. The root mean square fluctuations (RMSF) of residues in the F14 domain were analyzed throughout the trajectory (Fig. 10e). When the major residue fluctuations were compared between FHIP I (203–210) and FHIP II (216–235), it was observed that fluctuation in both the peptides were in the same range. The hydrogen bonding interaction between the protein and ligand throughout the simulation was analyzed. The number of hydrogen bonds between the protein and dodecasaccharide were constant for the complex with FHIP II whereas, for FHIP I complex the hydrogen bond number decreased (Fig. 10f) during the last 20 000 ps (30 to 50 ns). Hence, the molecular docking and MD simulation results show that the interaction of dodecasaccharide is stronger and stable with the FHIP II peptide in the F14 domain of FN.

Conclusions

Here, we have investigated the interaction of two peptides (FHIP I and FHIP II) of FN originating from domain III[14] of HEP II, which has important role in regulating FN function. Previously, FHIP I has been shown promoting focal adhesion assembly.[1] There, it was emphasized that specific sequence of FHIP I is a necessity for the underlined biological activity of FN. FHIP II can also contribute to heparin-binding owing to the presence of a basic amino acid cluster. In spite of so much interest, there is a lack of structural and thermodynamic information on the interaction of these peptide sequences with heparin. In the present paper, using a thorough experimental and simulation studies, we have tried to provide specified conclusions about the molecular basis of binding of these peptides with heparin.

Firstly, the observed binding affinities of FHIP I and FHIP II for heparin in this study are comparable to that of HEP II from where they originate.[10] Heparin is expected to interact with Arg and Lys of FHIP I or FHIP II that are found to be exposed on the surface of FN through ionic and H-bonding interactions. Thus, the much higher binding affinity of FHIP II ($\sim 10^7$ mol^{-1}) than FHIP I ($\sim 10^6$ mol^{-1}) (Tables 1 and 3) is due to its ability to form strong, specific H-bonding interactions using Arg and Lys residues with heparin, supported by the enthalpically driven binding in ITC. The results were further supported by the MD simulation data, which showed that the number of hydrogen bonds for heparin–FHIP II complex were constant throughout the simulation, whereas for FHIP I complex the hydrogen bond number decreased (Fig. 10f and S6†) towards the end of simulation. This is further buttressed by the existence of a positive ΔC_P for FHIP II, which indicates the burial of polar residues at the binding interface involved in specific H-bonding interactions. Earlier, similar studies on the binding of heparin with brain natriuretic peptide resulted in a positive ΔC_P. The study also concluded that H-bonding drove 94% of the interactions.[20] Several other proteins have been reported to form such specific interactions with heparin.[21,54]

Conversely, the interactions resulted in negative ΔC_P values for FHIP I at both the pHs. A negative ΔC_P is generally derived from the non-polar buried surface area, having strong implications in weak, hydrophobic interaction in complex formation.[5] Thus, the resultant FHIP I–heparin complex may have hydrophobic residues buried within its binding surface. The hydrophobic part in side chains of lysine and arginine can also contribute to the hydrophobic interactions with the heparin backbone. The hydrophobic parts of heparin are limited to the acetamide group (39), giving a narrow contribution to the binding. The heat capacity values are in a similar range as observed for other proteins binding to heparin.[55] Also, the observed pH dependent-binding of FHIP I or FHIP II can not be correlated with peptide sequence since Arg and Lys residues present in these sequences have pK_a much higher that the pH conditions used here. In fact, the lower affinity for either peptide at higher pH (Table 2) was attributed to weak helical structure of heparin as observed in CD (Fig. 5a).
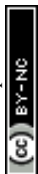
It can be concluded that FHIP I and FHIP II provide all the structural and thermodynamic elements necessary for binding of HEP II with heparin. The reasonably tight interaction between these peptides of FN and heparin may provide a clue about their biological role in cell adhesion activity, and allow the design of inhibitors or agonists of FN. Subsequently, it can be concluded that FHIP II could be a better location for therapeutic intervention in cell adhesion activity by FN.

Conflicts of interest

There are no conflicts to declare.

Acknowledgements

References

1 A. Woods, J. B. McCarthy, L. T. Furcht and J. R. Couchman, *Mol. Biol. Cell*, 1993, **4**, 605–613.

2 D. Missirlis, T. Haraszti, H. Kessler and J. P. Spatz, *Sci. Rep.*, 2017, **7**, 3711.

3 R. Pankov and K. M. Yamada, *J. Cell Sci.*, 2002, **115**, 3861–3863.

4 Y. Attieh, A. G. Clark, C. Grass, S. Richon, M. Pocard, P. Mariani, N. Elkhatib, T. Betz, B. Gurchenkov and D. M. Vignjevic, *J. Cell Biol.*, 2017, **216**, 3509–3520.

5 A. Sharma, J. A. Askari, M. J. Humphries, E. Y. Jones and D. I. Stuart, *EMBO J.*, 1999, **18**, 1468–1479.

6 K. L. Bentley, R. J. Klebe, R. E. Hurst and P. M. Horowitz, *J. Biol. Chem.*, 1985, **260**, 7250–7256.

7 X. Zhong, O. Arnolds, O. Krenczyk, J. Gajewski, S. Pütz, C. Herrmann and R. Stoll, *Biochemistry*, 2018, **57**, 6045–6049.

8 M. J. Benecky, C. G. Kolvenbach, D. L. Amrani and M. W. Mosesson, *Biochemistry*, 1988, **27**, 7565–7571.

9 M. Carpentier, A. Denys, F. Allain and G. Vergoten, *Glycoconjugate J.*, 2014, **31**, 161–169.

10 L. I. Gold, B. Frangione and E. Pearlstein, *Biochemistry*, 1983, **22**, 4113–4119.

11 G. Giancarlo, *Medicines*, 2019, **6**, 1–26.

12 I. Capila and R. J. Linhardt, *Angew. Chem., Int. Ed. Engl.*, 2002, **41**, 391–412.

13 M. Rusnati, D. Coltrini, P. Caccia, P. Dell'Era, G. Zoppetti, P. Oreste, B. Valsasina and M. Presta, *Biochem. Biophys. Res. Commun.*, 1994, **203**, 450–458.

14 T. Logue, M. Lizotte-Waniewski and K. Brew, *FEBS Lett.*, 2020, **594**(1), 94–103.

15 K. T. Yip, X. Zhong, N. Seibel, O. Arnolds, M. Schöpel and R. Stoll, *Biointerphases*, 2017, **12**, 02D415.

16 C. Tanmay, M. Mrinal, D. Ananya, B. Kalishankar, D. Ayan and M. K. Prasun, *J. Phys. Chem. B*, 2016, **120**, 2187–2197.

17 J. R. Fromm, R. E. Hileman, E. E. Caldwell, J. M. Weiler and R. J. Linhardt, *Arch. Biochem. Biophys.*, 1997, **343**, 92–100.

18 T. Goel, S. Kumar and S. Maiti, *Mol. BioSyst.*, 2013, **9**, 88–98.

19 E. Gonçalves, E. Kitas and J. Seelig, *Biochemistry*, 2006, **45**, 3086–3094.

20 R. E. Hileman, R. N. Jennings and R. J. Linhardt, *Biochemistry*, 1998, **37**, 15231–15237.

21 N. Tiwari, A. Srivastava, B. Kundu and M. Munde, *J. Mol. Recognit.*, 2018, 31.

22 J. B. McCarthy, M. K. Chelberg, D. J. Mickelson and L. T. Furcht, *Biochemistry*, 1988, **27**, 1380–1388.

23 J. L. Lau and M. K. Dunn, *Bioorg. Med. Chem.*, 2018, **26**, 2700–2707.

24 K. Hozumi, K. Nakamura, H. Hori, M. Miyagi, R. Nagao, K. Takasaki, F. Katagiri, Y. Kikkawa and M. Nomizu, *BioRes. Open Access*, 2016, **5**, 356–366.

25 N. Tanwar and M. Munde, *Int. J. Biol. Macromol.*, 2018, **112**, 1084–1092.

26 S. Gupta, N. Tiwari and M. Munde, *Sci. Rep.*, 2019, **9**, 5891.

27 G. Jones, P. Willett, R. C. Glen, A. R. Leach and R. Taylor, *J. Mol. Biol.*, 1997, **267**, 727–748.

28 N. M. O'Boyle, M. Banck, C. A. James, C. Morley, T. Vandermeersch and G. R. Hutchison, *J. Cheminf.*, 2011, **3**, 33.

29 H. J. C. Berendsen, D. van der Spoel and R. van Drunen, *Comput. Phys. Commun.*, 1995, **91**, 43–56.

30 V. Hornak, R. Abel, A. Okur, B. Strockbine, A. Roitberg and C. Simmerling, *Proteins*, 2006, **65**, 712–725.

31 A. W. Sousa da Silva and W. F. Vranken, *BMC Res. Notes*, 2012, **5**, 367.

32 J. E. Ladbury, J. G. Wright, J. M. Sturtevant and P. B. Sigler, *J. Mol. Biol.*, 1994, **238**, 669–681.

33 E. Ortiz-Salmerón, C. Barón and L. García-Fuentes, *FEBS Lett.*, 1998, **435**, 219–224.

34 A. Velazquez-Campoy, M. J. Todd and E. Freire, *Biochemistry*, 2000, **39**, 2201–2207.

35 N. R. Syme, C. Dennis, S. E. Phillips and S. W. Homans, *Chembiochem*, 2007, **8**, 1509–1511.

36 D. J. Samuel, P. Lauren, D. S. Matthew and C. J. Aaron, *J. Therm. Anal. Calorim.*, 2017, 127.

37 A. Basu, P. Jaisankar and G. Suresh Kumar, *Bioorg. Med. Chem.*, 2012, **20**, 2498–2505.

38 I. Haq, J. E. Ladbury, B. Z. Chowdhry, T. C. Jenkins and J. B. Chaires, *J. Mol. Biol.*, 1997, **271**, 244–257.

39 K. B. Kale and D. P. Ottoor, *Luminescence*, 2019, **34**, 39–47.

40 A. Biswas, R. K. Swarnkar, B. Hussain, S. K. Sahoo, P. I. Pradeepkumar, G. N. Patwari and R. Anand, *J. Phys. Chem. B*, 2014, **118**, 10035–10042.

41 R. Cerpa, F. E. Cohen and I. D. Kuntz, *Folding Des.*, 1996, **1**, 91–101.

42 C. A. Fitch, G. Platzer, M. Okon, B. E. Garcia-Moreno and L. P. McIntosh, *Protein Sci.*, 2015, **24**, 752–761.

43 S. Patel, A. F. Chaffotte, B. Amana, F. Goubard and E. Pauthe, *Int. J. Biochem. Cell Biol.*, 2006, **38**, 1547–1560.

44 U. Anand, C. Jash and S. Mukherjee, *J. Phys. Chem. B*, 2010, **114**, 15839–15845.

45 L. Jendeberg, M. Tashiro, R. Tejero, B. A. Lyons, M. Uhlén, G. T. Montelione and B. Nilsson, *Biochemistry*, 1996, **35**, 22–31.

46 M. Goodman and C. Toniolo, *Biopolymers*, 1968, **6**, 1673–1689.

47 R. C. Hider, G. Kupryszewski, P. Rekowski and B. Lammek, *Biophys. Chem.*, 1988, **31**, 45–51.

48 H. Lin, R. Lal and D. O. Clegg, *Biochemistry*, 2000, **39**, 3192–3196.

49 Sachchidanand, O. Lequin, D. Staunton, B. Mulloy, M. J. Forster, K. Yoshida and I. D. Campbell, *J. Biol. Chem.*, 2002, **277**, 50629–50635.

50 D. Carstanjen, P. Dutt and T. Moritz, *J. Virol.*, 2001, **75**, 6218–6222.

51 R. M. Srikumar, R. S. Satinder, C. Amitabha and L. K. Anil, *Biophys. J.*, 1999, **76**, 1469–1479.

52 J. Schiebel, R. Gaspari, T. Wulsdorf, K. Ngo, C. Sohn, T. E. Schrader, A. Cavalli, A. Ostermann, A. Heine and G. Klebe, *Nat. Commun.*, 2018, **9**, 3559.

53 N. T. Truc, V. M. Hoang and L. S. Mai, *Sci. World J.*, 2014, **2014**, 1–14.

54 H. V. Patel, A. A. Vyas, K. A. Vyas, Y. S. Liu, C. M. Chiang, L. M. Chi and W. Wu, *J. Biol. Chem.*, 1997, **272**, 1484–1492.

55 D. Chandler, *Nature*, 2002, **417**(6888), 491.